



Rocking-Chair Configuration in Ultrathin Lithium Vanadate-Graphene Hybrid Nanosheets for Electrical Modulation

Haiou Zhu¹, Xinming Qin², Xu Sun¹, Wensheng Yan³, Jinlong Yang² & Yi Xie¹

¹Division of Nanomaterials and Nanochemistry, Hefei National Laboratory for Physical Sciences at the Microscale, University of Science and Technology of China, Hefei, Anhui, 230026, P. R. China, ²Theoretical and Computational Sciences, Hefei National Laboratory for Physical Sciences at Microscale, University of Science and Technology of China, Hefei, Anhui, 230026, P. R. China, ³National Synchrotron Radiation Laboratory, University of Science and Technology of China, Hefei, Anhui 230029, P.R. China.

SUBJECT AREAS:
ELECTRONIC DEVICES
GRAPHENE
NANOSCALE DEVICES
NANOSCALE MATERIALS

Received
29 November 2012

Accepted
25 January 2013

Published
13 February 2013

Correspondence and
requests for materials
should be addressed to
Y.X. (yxie@ustc.edu.
cn)

The ability to control electronic property of a material by externally applied voltage is greatly anticipated in modern electronics, and graphene provide potential application foreground for this issue on account of its exotic ambipolar transport property. In this study, we proposed that inorganic-graphene intercalated nanosheet is an effective solution to optimize the transport property of graphene. As an example, lithium vanadate-graphene (LiVO-graphene) alternately intercalated nanosheets were designed and successfully synthesized. Theoretical calculation implied that its rocking chair configuration may provide a new pathway to switch the carrier in graphene layer between p-type and n-type while the position of embedded Li ions is controlled by an external field. Thus, a demo transistor was fabricated with layer-by-layer overlapping of LiVO-graphene nanosheets which proved that this inorganic-graphene structure could be used for electrical modulation in electronic devices.

Effective manipulating the electronic structure of any given material is always being an attractive issue for scientists and engineers for the huge potential applications. Materials with precisely manipulated electronic structure could be used to assemble electronic devices, and the ability to control electrical property of a material by externally applied voltage is at the heart in modern electronics. However, the electronic structure of conventional material is fixed and hard to control for their fixed crystalline structure. Recently, graphene attracted much attention due to its possibility to provide potential solution for this issue^{1,2}.

Graphene, a monolayer of carbon atoms tightly bonded together with σ bonds, and with a π orbital perpendicular to the plane in each carbon atom in the lattice, has many exotic physical properties, such as high intrinsic carrier mobility, ambipolar field effect and anomalous quantum Hall Effects. The valence band and conduction band of graphene touch each other at the six corners of the 2D Brillouin zone, and the energy of Fermi level belongs to both bands. Due to the unique band structure, the carriers in the graphene are bipolar, and thus the charge carriers can change from electrons (n-type) to holes (p-type) with the application of an external electric field³⁻⁶. All the above properties enable graphene sheets as the most promising candidate material for hybrid nanocomposites based electronic devices. However, graphene based electronic devices has their own disadvantages due to the ambipolar transport property, through which the charge carriers can easily change from electrons to holes with the application of an electrostatic gate, therefore, the electrical modulation efficiency is scant for its relatively high leakage current in electronic devices. Currently, high leakage current in graphene-based transistors can be addressed through band gap engineering, i.e. open energy gap of graphene to decrease the leakage current (I_{off}), but in turn results in degraded mobility. Decreasing of carrier mobility leads to a reduced conductivity and a lack of sufficient drain current saturation (I_{on})⁷⁻¹³. On the other hand, the transport property of the graphene could be significantly altered by introducing dopants to the graphene. There have been many reports concerning this issue by adsorbing different molecules to graphene, and these molecules may act as electron acceptors or electron donors to graphene when interact with graphene, inducing remarkable change to the electronic structure of graphene, thus alter the transport property of graphene ulteriorly¹⁴⁻¹⁷. Here, we proposed that inorganic-graphene alternately intercalated nanosheets should be an effective solution to optimize the transport property of graphene.

As it is known, many vanadium oxides tend to form lamellar structure, and lithium vanadate was chosen as the host material for intercalation in this study. As an example, $Li_{1.2}V_{3.34}O_{7.34} \cdot 2H_2O$ (abbreviated as LiVO thereafter)



is a compound which has lamellar structure with square pyramidal coordination for vanadium¹⁸, in which the vanadium oxide sheets are planar, and lithium ion can reversibly intercalate into the vanadium oxide sheets, making it candidate for cathode in lithium ion batteries. Polyethylene oxide has been reported to intercalate between vanadium oxide layers, which confirmed the reliability for intercalating lamella material into the vanadium oxide framework in $\text{Li}_{1.2}\text{V}_{3.34}\text{O}_{7.34}\cdot 2\text{H}_2\text{O}$ ¹⁹. In this study, we synthesized LiVO-graphene intercalated compound for the first time, in which the layers of lithium vanadate were alternately intercalated with graphene. The LiVO-graphene was then peeled off into mono- or few-layered LiVO-graphene ultrathin nanosheets. The quasi-lithium ion battery configuration of LiVO-graphene ultrathin nanosheets reminds us that the embedded lithium ions may response to the external electric field by rocking back and forth between vanadium oxide (abbreviated as VO thereafter) layer and the graphene layer, and then reversibly alter the electronic structure of graphene, providing a perfect alternative for improvement of the electrical modulation property of graphene-based electronic devices.

Results

In this study, the new layered compound of LiVO-graphene was obtained by a solvothermal method using VCl_3 , LiNO_3 , $\text{LiOH}\cdot\text{H}_2\text{O}$ and previously prepared graphene as the raw materials as presented in **Figure 1a and 1b** (details presented in Experimental section). The crystal structures of the LiVO-graphene and the pure LiVO were investigated using X-ray powder diffraction (XRD) respectively (**Figure 1c**). All of the peaks for pure LiVO could be readily indexed to $\text{Li}_{1.2}\text{V}_{3.34}\text{O}_{7.34}\cdot 2\text{H}_2\text{O}$ with tetragonal lattice. The XRD pattern with the presence of graphene have most peaks similar with LiVO except for the appearance of a strong new diffraction peak with the d spacing of about 12.5Å, and a weak second order diffraction peak with the d spacing of about 6.25Å further confirmed the

formation of a new d-spacing of 12.5Å for the new layered compound with the new interlayer periodicity of 12.5Å.

The high-resolution transmission electron microscope (HRTEM) images of the LiVO-graphene gave the microscopic structural information as shown in **Figure 1d**. The lattice spacing of 12.5Å is detected to match with the new-formed interlayer distance of LiVO-graphene. The HRTEM images further confirmed the intercalation of graphene layer into VO layer, which increased the d(002) from 7.9 Å to 12.5 Å. Compared with the d-spacing of (002) plane in LiVO, the new-formed interlayer distance is 4.6Å larger than that in pure LiVO, which can be assigned to the intercalation of monolayer graphene. So, the periodicity of 12.5 Å is roughly the sum of the layer spacing of lithium vanadate and graphene, suggesting that the monolayer graphene alternately intercalates into the adjacent VO layers. The X-ray photoelectron spectroscopy (XPS) spectra (**Figure S2**), the energy dispersive X-ray spectroscopy (EDS) spectra (**Figure S3**) and the near edge X-ray absorption fine structure (NEXAFS) spectra of pure LiVO, LiVO-graphene and graphene (**Figure S4**) were recorded respectively, which further confirmed that the both the graphene and LiVO layer kept intact during the intercalation process except for widening of d-spacing along c-axis direction as a result of graphene intercalation. Based on the crystallographic structure of parent compound $\text{Li}_{1.2}\text{V}_{3.34}\text{O}_{7.34}\cdot 2\text{H}_2\text{O}$ (**Figure S1a**), the intercalated LiVO framework could be suggested as shown in **Figure S1b**. The simulated XRD pattern of the suggested intercalated LiVO framework was presented in **Figure 1c**, in which the peaks match well with new peaks arising after intercalation, indicating that the suggested structure of the new LiVO framework is coincident with the actual situation. The schematic crystal structure of LiVO-graphene projected along c axis was shown in **Figure 1b**. The selected-area electron diffraction (SAED) shown in **Figure 1d** confirmed that LiVO-graphene nanosheets are polycrystalline due to the intercalation of monolayer graphene, and the polycrystalline diffraction rings are exactly indexed to the intercalated LiVO-graphene as presented in **Figure S1** and the

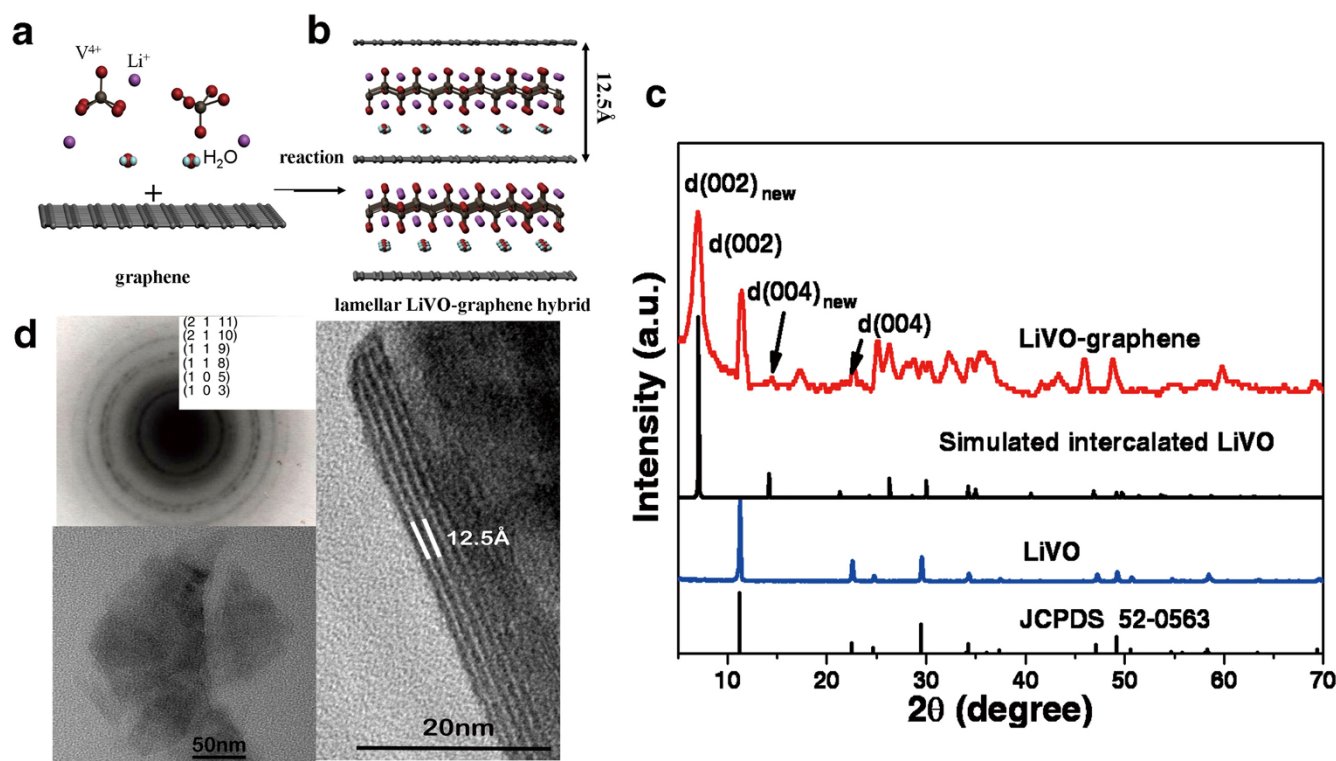


Figure 1 | Characterization of as-obtained intercalated LiVO-graphene. (a,b) The sketch map of the reaction process in the fabrication of intercalated LiVO-graphene nanosheets. (c) XRD patterns of the as-prepared lithium vanadate-graphene (LiVO-graphene), simulated new intercalated LiVO framework, pure LiVO and XRD standard pattern of LiVO. (d) HRTEM image and the SAED pattern of LiVO-graphene.



d-spacings in the SAED pattern match well with the simulated XRD pattern of intercalated LiVO, further confirming the structure of the intercalated LiVO-graphene.

It has been clearly confirmed that LiVO-graphene is a new layered structure stacked by VO-graphene-lattice water alternating layers, and the weak Van der Waals interlayer interactions presented among the layers bring exfoliative characteristic to this compound. The exfoliation efficiency comparison test was done in various solvents, and finally H₂O show the best exfoliation efficiency as shown in Figure S6, which could be attributed to the strong hydrogen bonding interaction between H₂O in solvent and the lattice H₂O molecules in the LiVO-graphene compound. The hydrogen bonding interaction promoted the exfoliation process, and the resultant exfoliated LiVO-graphene nanosheets were successfully obtained. Macroscopically, a well defined Tyndall effect was observed in the translucent suspension of LiVO-graphene, indicating the presence of highly exfoliated LiVO-graphene layers in water, as shown in Figure S7²⁰. AFM analysis of the exfoliated LiVO-nanosheets revealed that the sample was mainly composed of ultrathin nanosheets of LiVO-graphene (Figure S7), matching well with the thickness of LiVO-graphene nanosheets.

The exfoliated LiVO-graphene ultrathin nanosheets have a representative structure similar to micro-lithium ion battery with the LiVO layer as cathode electrode and graphene layer as the anode electrode. This interesting quasi-lithium ion battery structure reminds us that Li ions embedded between the LiVO layer and the graphene layer may move back and forth in response to an external electric field perpendicular to the nanosheets, thereby altering the charging carriers of the graphene layer, and ultimately changing the transport characteristic of the nanosheets. Based on this assumption,

a pair of LiVO-graphene layer was taken for calculation (details see experimental section) to better understand the various electronic structures with different Li ion position.

First, crystallography analysis of pure LiVO gives the distance between V and Li atom ($d_{\text{Li-V}}$) for the primitive position of lithium ion is 2.28 Å (Figure 2a). Further more, the accurate position of the intercalated graphene layer can be estimated by calculating the total energy with different vertical graphene-O distance ($d_{\text{graphene-O}}$, Figure 2a) as shown in Figure S8, revealing that the equilibrium distance of $d_{\text{graphene-O}}$ is 2.9 Å. The electronic structure of each part of the LiVO-graphene nanosheet was considered separately. Taking the LiVO layer into first consideration, the densities of states (DOS) structure of LiVO layer was calculated as presented in Figure S9, indicating that LiVO layer is always n-type carrier no matter what position the embedded Li ions occupy. However the electronic structure of the graphene layer is greatly affected by the position of the embedded Li ions. It is known that in graphene, the (s, p_x, p_y) orbitals of carbon atom combine to form the σ (bonding) and σ^* (anti-bonding) orbital, which are well separated in energy, thus are too far away from the Fermi level to influence the electronic property of graphene, so these orbitals are frequently neglected when concerning the electronic property. Only the remaining p_z (π) orbitals lie in the vicinity of the Fermi level, therefore p_z orbitals of carbon atom are considered independently to describe electronic property of graphene in this study^{21–23}. The projected density of states (PDOS) of carbon p_z orbital for the graphene layer with different Li ion position was calculated separately, in which the energy where the conduction band and the valence band meet is the energy of Dirac point for graphene (abbreviated as E_{dg} thereafter). In the case of Li ions at their original

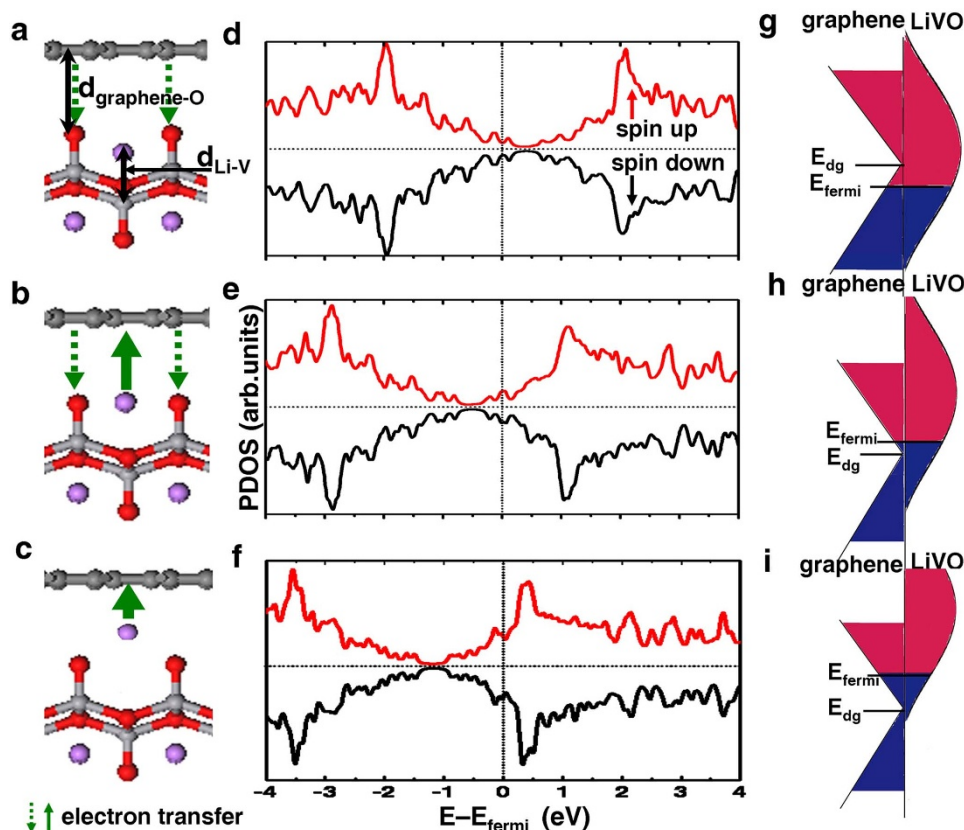


Figure 2 | The projected density of states (PDOS) of the carbon p_z orbital for graphene and electron transfer process in different conditions.

(a, b, c) The sketch maps of charge transfer process between the graphene layer and the VO layer at the condition: (a) $d_{\text{Li-V}} = 2.28 \text{ \AA}$, (b) $d_{\text{Li-V}} = 3.0 \text{ \AA}$, (c) $d_{\text{Li-V}} = 3.8 \text{ \AA}$ respectively. (d, e, f) PDOS of carbon p_z orbital for graphene at the condition: (d) $d_{\text{Li-V}} = 2.28 \text{ \AA}$, (e) $d_{\text{Li-V}} = 3.0 \text{ \AA}$, (f) $d_{\text{Li-V}} = 3.8 \text{ \AA}$, respectively. (h, i, j) electron-transfer mechanism within the Marcus-Gerischer theory: right, schematic of LiVO layer density of states (DOS); left: graphene layer DOS at the condition: (h) $d_{\text{Li-V}} = 2.28 \text{ \AA}$, (i) $d_{\text{Li-V}} = 3.0 \text{ \AA}$, (j) $d_{\text{Li-V}} = 3.8 \text{ \AA}$, respectively.



position ($d_{\text{Li-V}}$ value is 2.28\AA when $V_G = 0\text{ V}$), the PDOS of carbon p_z orbital (Figure 2d) indicate that E_{dg} lies above the Fermi level of LiVO-graphene system (as abbreviated as E_{fermi}), implying that there is a driving force to shift the Fermi level of LiVO-graphene system into the valence band of graphene (Figure 2g), and this transfer can be further explained as follows: O atom, which lies at the top of the VO layer, is a stronger electron-withdrawing group compared to graphene layer, since graphene is neither a strong electron donor nor a strong acceptor due to its ambipolar nature, thus the O atoms can withdraw electrons from the graphene layer, as a result, electrons flow from the graphene layer to the VO layer until equilibrium is reached (Figure 2a), and finally the electrochemical potential of the graphene layer and the lithium vanadate layer are aligned. The electron transfer trajectory revealed that the graphene layer at this state is p-type carrier. However, carrier type of graphene layer will change if the Li ions are pushed to the graphene layer by the external field. Taking $d_{\text{Li-V}} = 3.0\text{\AA}$ for example, at which the Li ions are on the same plane with the top O atoms of VO layer along c axis, the E_{dg} of graphene lies slightly below E_{fermi} (Figure 2e), revealing that a weak driving force shifting the Fermi level into the conduction band of graphene^{24,25}. Accordingly, the schematic diagram of electron transfer in Figure 2b revealed that when $d_{\text{Li-V}} = 3.0\text{\AA}$, partly ionized Li atoms move close to the graphene layer, then two types of competitive interlayer electron transfer trajectory coexist: the electrons transfer from partly ionized Li ions to the graphene layer, and the electrons transfer from the graphene layer to O atom at the top of the VO layer, between which the former one plays the dominant role. Partly ionized lithium atom is an electron-donating group, so electrons flow from VO layer to graphene layer. This electron transfer trajectory reveals that graphene layer at this state is n-type carrier. If the Li ions are pushed further to the graphene layer, taking $d_{\text{Li-V}} = 3.8\text{\AA}$ for another example as presented in Figure 2f, the E_{dg} of graphene layer lies far above E_{fermi} , and a strong driving force shifts the Fermi level to the conduction band of graphene (Figure 2j), which is similar to the former case in Figure 2h, and thus graphene layer at this state is also n-type carrier. Above calculations reveal that the position of Li ions may play a crucial role in determining the carrier type of graphene layer in LiVO-graphene. At the original state of $d_{\text{Li-V}}$ is 2.28\AA , the carrier type for graphene layer is p-type, and the

VO layer is an n-type carrier all the time, so the inner p-n junction may form. When the Li ions are pushed to the position with the $d_{\text{Li-V}}$ is 3.0\AA , the graphene layer changes to be n-type carrier too and thus the inner p-n junction may disappear.

The consideration that the position of Li ions may be controlled by external electric field on the analogy of the lithium ion batteries, combining with the verdict mentioned above, gives us the inspiration that the LiVO-graphene nanosheets may be assembled into a demo device for electrical modulation with the application of an external electric field. A simple demo transistor was thus designed based on the consideration hereinbefore and then fabricated via the assembly with layer-by-layer overlapping of exfoliated nanosheets (details presented in the experimental section and the simplified configuration presented in Figure 3a). It should be noted that the assembly quality of the layer-by-layer overlapping structure greatly influenced the output transport characteristic of the demo transistor. In the as-fabricated transistor, source and drain electrodes were applied for transport measurement while the external electric field (V_G) was supplied by a direct current (DC) electrical source between the top gate and the silicon back gate. In this study, drain-source current (I_{ds}) versus drain-source voltage (V_{ds}) presented the output characteristics of the transistor at various V_G voltage of 0 V, 0.5 V, 1 V, 3 V, as presented in Figure 3b, respectively. The device shows on current (I_{on}) of 2.25 mA ($V_{\text{ds}} = 1.6\text{ V}$ and $V_G = 3\text{ V}$), and off current (I_{off}) of 0.107 mA ($V_{\text{ds}} = 1.6\text{ V}$ and $V_G = 0\text{ V}$), from which we can clearly see that the positive current increases remarkably by increasing the voltage of the external electric field, and the negative current remains at very small value with little change while increasing the external electric field. An $I_{\text{on}}/I_{\text{off}}$ ratio of 21 (2.250 mA/0.107 mA) was obtained in this demo transistor, showing significant improvement over the existing reports in full consideration of the $I_{\text{on}}/I_{\text{off}}$ ratio, I_{on} and I_{off} parameters^{26–28}.

Discussions

It is easy to understand that embedded Li ions could be readily moved between the neighboring VO layer and graphene layer under external electric field, which is similar to the charging/discharging process in rocking chair configuration of lithium ion battery. The transport characteristics of the transistor perfectly tallies with the

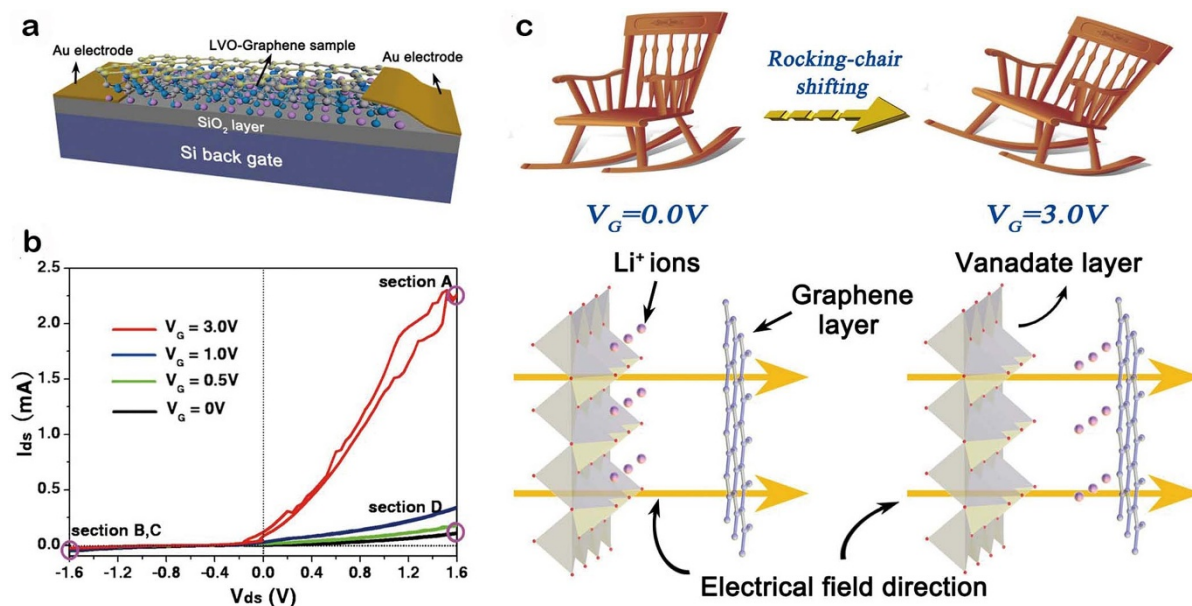


Figure 3 | Schematic representation of the structure and the transport poverty of the demo transistor. (a) The simplified configuration of the LiVO-graphene based transistor. (b) The V_{ds} as a function of I_{ds} curve of the transistor with different V_G value. V_G is the applied external field voltage perpendicular to the film. (c) The sketch map of the rocking-chair ion polarization in monolayered LiVO-graphene nanosheet.



summing-up hereinbefore: the embedded Li ions move approach the LiVO layer when $V_G = 0$ V, thus the graphene layer is p-type carrier and an inner p-n junction exists in the nanosheets therefore a low current (I_{off}) can be achieved in the device; while $V_G = 3$ V, the embedded Li ions move near to the graphene layer, shifting the graphene layer to be n-type carrier, the p-n junction disappears to achieve a high I_{on} state for electrical modulation purpose (Figure 3c). That is the basic principle for the LiVO-graphene based transistor.

The detailed explanation for the actual LiVO-graphene based transistor is further presented in Figure 4, in which different situations are brought forward according to the measurement condition. In all the cases, the external electric field added on the top and back gates and the electronic flow between the S and D contacts work synergistically on determining the transport efficiency of the film. When the existed external electric field V_G is 3 V, which is high enough to push the Li ions move to the graphene layer (d_{Li-V} is 3.8\AA for example), electrons transfer from Li atoms to graphene layer, and then the electronic flow between the D and S contact ($-I_{ds}$) plays a critical role in determining the transport efficiency: when V_{ds} is positive, the direction of electronic flow is the same with the electron transfer direction as shown in Figure 4c, and as a result, the current flow is highly enhanced (section A in Figure 3b and Figure 4s), which can explain the high I_{on} value of the LiVO-graphene based transistor. Otherwise, when the voltage between the D and S contact (V_{ds}) is negative, the electronic flow is in the opposite

direction of electron transfer, as presented in Figure 4d, thus the electronic flow is inhibited by the opposite electron transferring process from Li atoms to the graphene layer, resulting in a low current flow (section B in Figure 3b and Figure 4d). In the case without external gate voltage ($V_G = 0$ V), when the Li atoms remain at their original position without polarization ($d_{Li-V} = 2.28\text{\AA}$), there is weak electron transfer from the graphene layer to O atoms as shown in Figure 4e, here the graphene layer is p-type carrier, and the inner p-n junction exists no matter what current direction was between the S and D contact, and furthermore this stacking p-n junctions form a p-n-p-n-..... junction, resulting in the increased width of the depletion zone whatever the direction of V_{ds} is, thus the current flow (I_{ds}) is always very weak (section C and D in Figure 3b and Figure 4e). This is the reason of lower I_{off} value in the LiVO-graphene based transistor.

Of course, the exfoliated product of the LiVO-graphene precursor may be not only monolayered LiVO-graphene hybrid nanosheets ideally, some other hybrid nanosheets with different compositions, such as LiVO-graphene-LiVO or graphene-LiVO-graphene and so on, may co-exist with monolayered LiVO-graphene hybrid nanosheets due to the varying exfoliation degrees. Furthermore, the ideally layer-by-layer overlapping of LiVO-graphene nanosheets with the same stacking direction (as shown in Figure 4b) is difficult to practically control. But the theoretical analyses in Figure S10 and Figure S11 suggest that only monolayered LiVO-graphene

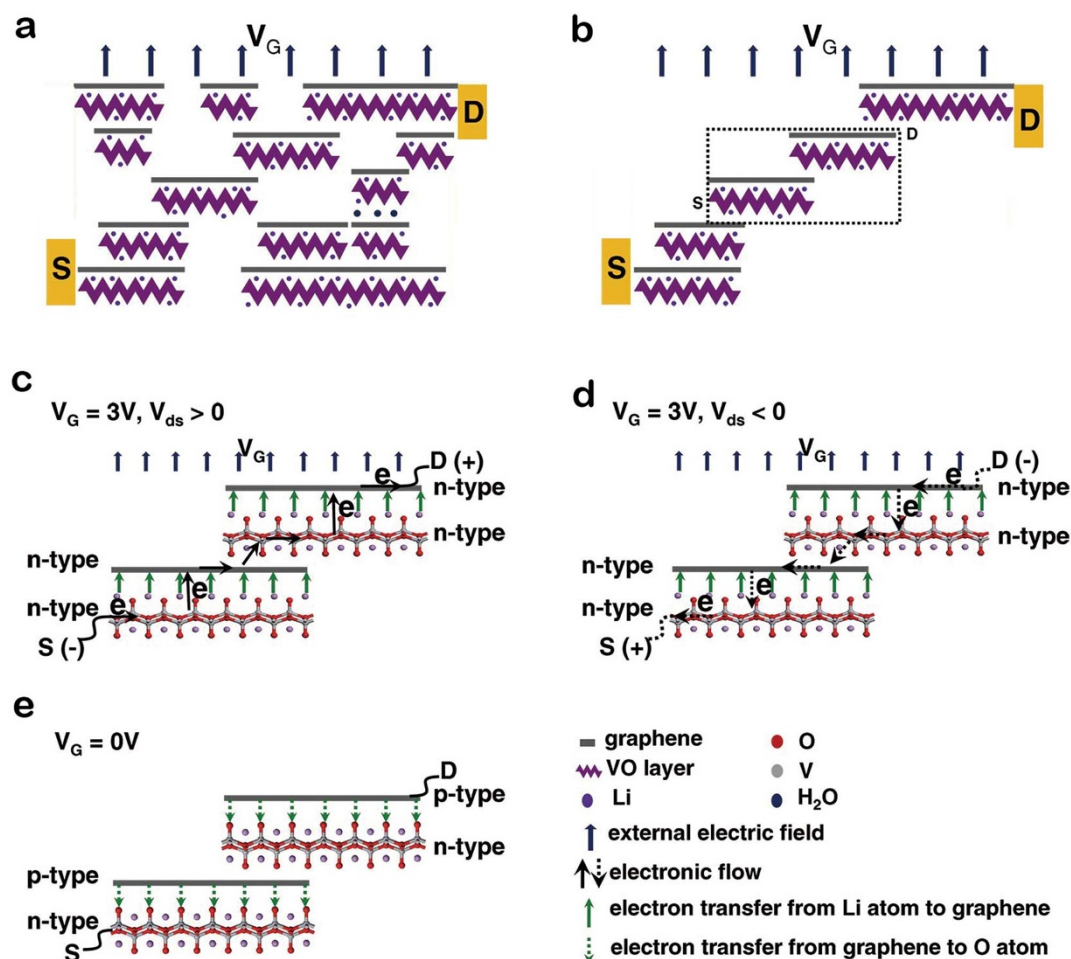


Figure 4 | Microscopic schematic view of the demo transistor and probable electronic channels. (a) Microscopic schematic view of transistor with layer-by-layer overlapping of LiVO-graphene nanosheets. (b) Probable electronic channels of current flow in the transistor. (c) at $V_G = 3$ V and $V_{ds} > 0$, the current is enhanced since the electronic flow (black arrows) has the same direction with that of electron transfer (green arrows) from Li atoms to graphene. (d) at $V_G = 3$ V and $V_{ds} < 0$, the current is decreased since the electronic flow (black arrows) has the opposite direction with electron transfer (green arrows) from Li atoms to graphene. (e) $V_G = 0$ V, a lower I_{off} is achieved since the inner p-n-p-n-..... junction forms.



nanosheets overlapping with the same stacking direction contribute to the transistor. So despite the possible existence of the LiVO-graphene-LiVO and graphene-LiVO-graphene nanosheets in the exfoliated nanosheets product and also possible coexistence of the opposite stacking direction for the monolayered LiVO-graphene nanosheets overlapping, neither of them contribute to the transport property of the transistor, since the electronic channels would be cut off no matter whether the external electric field exists or not in these cases.

Briefly, based on the quasi-lithium ion battery mechanism, the current flow between S and D (I_{ds}) change with the external electric field (V_G) and voltage between S and D (V_{ds}) can be easily understood: the altering of V_G changes the position of the embedded Li ions between the graphene layer and VO layer, thus switches the carrier type of the graphene layer, and at the same time the layer-by-layer overlapping structure of LiVO-graphene nanosheets is requisite for the formation of a electronic flow channel in transistor. The peculiar transistor character is the result of the synergetic effect of the external electric field and the electronic flow between the S and D contacts. The quasi-rocking chair configuration enables this demo transistor differs from the graphene-made transistor reported before: an inner p-n junction exists in the obtained LiVO-graphene alternately intercalated nanosheets when the external electric field is removed, which finally decrease the leakage current (I_{off}) in the transistor. Meanwhile the drain current (I_{on}) can be increased by introducing a neighboring intercalated layer to provide the graphene layer with sufficient electron carriers. Although the demo transistor is roughly constructed at current stage, the underlain principle confirms us that the rocking chair configuration of such monolayered intercalated hybrid nanosheets may provide a new pathway to effectively manipulate the transport property of graphene.

To conclude, a novel LiVO-graphene alternately intercalated hybrid was synthesized for the first time and then exfoliated into ultrathin nanosheets. The calculation of electronic structure of LiVO-graphene with different Li ion position revealed that the carrier type of the graphene layer could be altered by rocking the embedded Li ions back and forth with the application of external electric field. The rocking chair configuration of LiVO-graphene alternately intercalated nanosheets may provide a new way for electrical modulation. Based on this idea, a simple demo transistor was designed and assembled with layer-by-layer overlapping of the LiVO-graphene alternately intercalated nanosheets, and the following I-V characteristic revealed that the resistance of the LiVO-graphene film could be controlled by the applied external electric field, which gave a direct evidence for our initial idea, *i. e.* the electronic structure could be altered by the external electric field, and as a result, a inner p-n junction existed or disappeared accordingly. The integration of inner p-n junction produced in the alternately intercalated inorganic-graphene hybrid perfectly fulfilled the demand for micro miniaturization of new generation of nanoelectronics, revealing potential application foreground in nanoelectronic devices for electrical modulation purpose.

Methods

Preparation of graphene. In a typical procedure, graphite oxide was prepared from purified natural graphite by the modified Hummers method²⁹. After fully oxidation, the residual salts and acid were removed, then 3 mmol of the obtained graphite oxide was ultrasonicated in 100 ml water for over 1 h to get graphene oxide (GO) collosol until it became clear with no visible particles, and then the collosol was transferred to a 250 ml round-bottom flask, followed by 0.031 ml hydrazine hydrate (85%) and 0.784 ml ammonia solution (25%) adding into the flask under stirring. And then the solution was heated in an oil bath at 100 °C under a water-cooled condenser for 24 hours, and finally the as-obtained graphene black collosol was cooled for further intercalation. Raman spectroscopy was measured to characterize graphene as shown in Figure S5. The Raman spectroscopy showed that the as-obtained graphene is defective.

Preparation of LiVO-graphene and LiVO. The obtained graphene mentioned above was exfoliated and dispersed under ultrasonic treatment for several hours to break the

large and thick graphene into small and thin pieces, the exfoliated graphene solution was obtained for the following use: 0.40 mmol VCl_3 and 0.46 mmol lithium nitrite ($LiNO_2$) were dissolved into 31 ml benzyl alcohol, stirred for 5 minutes, then 2 ml LiOH (0.5 mM) were added to form suspension with a ball of yellow floccules after ultrasonic irradiation for several minutes. After that, 3 ml graphene collosol was dropped into the flask to form well-distributed suspension. The total volume of the suspension was transferred into a 40 ml stainless Teflon-lined autoclave. The autoclave was heated to 200 °C at the heating rate of 5 °C min^{-1} and maintained at 200 °C for 24 hours. The reaction system was cooled to room temperature in air. The obtained dark green deposition was collected by centrifugation at 10000 rpm for 2 minutes, and then washed with cyclohexane, dried under vacuum at 60 °C for 8 hours. The final lithium vanadate-graphene powders are collected.

For comparison, pure lithium vanadate $Li_{1.2}V_{3.34}O_{7.34} \cdot 2H_2O$ was prepared according to the former steps without addition of graphene.

Exfoliation of LiVO-graphene into LiVO-graphene nanosheets. 10 mg above-obtained lithium vanadate-graphene compound was dispersed in 20 ml water in a beaker, and followed by the dispersion ultrasonicated for 10 minutes. Then the resultant lithium vanadate-graphene suspension was further exfoliated into small and thin pieces. The exfoliated suspension was then centrifuged for several minutes and the superstratum liquid with ultrathin nanosheets was collected for the device assembly.

Assembly of LiVO-graphene nanosheets into transferable thin films. The LiVO-graphene ultrathin nanosheets suspension was then vacuum-filtrated over a piece of micropored cellulose membrane with 0.22 μm pore size to form a homogeneous thin film, of which the thickness can be controlled by changing the filtrated amounts of the nanosheet suspension (Figure S12).

Fabrication of transistor with LiVO-graphene film. The prototype device of the lithium vanadate-graphene nanosheet-based transistor was fabricated. In briefly, the LiVO-graphene film was transferred onto Si/SiO₂ wafers. The p-doped Si substrate under a dielectric SiO₂ layer (300 nm) was used as the back gate. The micropored cellulose membrane was then dissolved in acetone. Two Au charge collectors were sprayed onto the top of the hybrid film and extended to cover the section of the LiVO-graphene film to form Ohmic contacts and act as the source (S) and drain (D) contacts for electron transport measurement. To obtain a uniform external electric field, Ag film was used as the top gate. Although the LiVO-graphene films are too large in size (10 mm*6 mm*5 μm) for practical devices, this device configuration is sufficient for principle demonstration.

Sample characterization. The phase structure of the product was characterized using X-ray powder diffraction (XRD) with Philips X'Pert Pro Super diffractometer with Cu K_α radiation ($\lambda = 1.54178 \text{ \AA}$). The field emission scanning electron microscopy (FESEM) images were obtained by JEOL JSM-6700F scanning electron microscopy. The transmission electron microscopy (TEM) images were taken on Hitachi H-800 transmission electron microscopy at an acceleration voltage of 200 kV. High resolution transmission electron microscopy (HRTEM) images were taken by JEOL-2010 transmission electron microscopy at an acceleration voltage of 200 kV. Raman spectrum was taken on a SPEX 1403 spectrometer with Ar⁺ laser at an excitation wavelength of 514.5 nm. The XPS spectrum was taken by VEGESCALAB MKIIX-ray photoelectron spectrometer with an exciting source of Al K_α. Atomic force microscopy (AFM) measurement was performed by the Veeco di-Innova Scanning Probe Microscopy. Electrochemical performance of the transport measurement of the dual-gated FET was studied by cyclic voltammetry (CV) at an electrochemical station (CHI660B).

Calculations. The electronic structure of LiVO-graphene was calculated by employing the Vienna ab initio simulation package (VASP)^{30,31} with the projector augmented plane wave method³². The local density approximation (LDA) was chosen for it can get good interlayer separations^{33,34}. The on-site correction has been applied to the 3d electron of V atoms by $L(S)DA + U^{35}$, the values of U is 3.4 eV³⁶. The energy cutoff of 400 eV and the Monkhorst-Pack mesh of k-points samples in two-dimensional Brillouin zone with 2*8*1 points were applied. The LDA lattice parameter for graphene is $a = 2.446 \text{ \AA}$, and monolayer graphene with 72 carbon atoms is used to match a 7*2 LiVO layer. The supercell contains 170 atoms (25.42*7.34*20 \AA^3), and the vacuum space perpendicular to the LiVO-graphene slab is 12 \AA , which is enough to ignore the interaction between periodic images. A dipole correction to avoid interactions between periodic images along the c direction was also adopted³⁷.

1. Zhang, Y. B. *et al.* Direct observation of a widely tunable bandgap in bilayer graphene. *Nature* **459**, 820–823 (2009).
2. Novoselov, K. S. *et al.* Electric Field Effect in Atomically Thin Carbon Films. *Science* **306**, 666–669 (2004).
3. Ohta, T., Bostwick, A., Seyller, T., Horn, K. & Rotenberg, E. Controlling the Electronic Structure of Bilayer Graphene. *Science* **313**, 951–954 (2006).
4. Zhu, Y. W. *et al.* Graphene and Graphene Oxide: Synthesis, Properties, and Applications. *Adv. Mater.* **22**, 3906–3924 (2010).



5. Xia, F. N., Farmer, D. B., Lin, Y. M. & Avouris, P. Graphene Field-Effect Transistors with High On/Off Current Ratio and Large Transport Band Gap at Room Temperature. *Nano Lett.* **10**, 715–718 (2010).
6. Williams, J. R., DiCarlo, L. & Marcus, C. M. Quantum Hall Effect in a Gate-Controlled p-n Junction of Graphene. *Science* **317**, 638–641 (2007).
7. Meric, I. *et al.* Current saturation in zero-bandgap topgated graphene field-effect transistors. *Nat. Nanotechnol.* **268**, (2008).
8. Chen, Z. H., Lin, Y. M., Rooks, M. J. & Avouris, P. Graphene nano-ribbon electronics. *Physica E*. **40**, 228–232 (2007).
9. Li, X. L., Wang, X. R., Zhang, L., Lee, S. W. & Dai, H. J. Chemically Derived, Ultrasmooth Graphene Nanoribbon Semiconductors. *Science* **319**, 1229–1232 (2008).
10. Han, M. Y., Ozyilmaz, B., Zhang, Y. B. & Kim, P. Energy Band-Gap Engineering of Graphene Nanoribbons. *Phys. Rev. Lett.* **98**, 206805 (2007).
11. Schwierz, F. graphene transistors. *Nat. Nanotechnol.* **5**, 487–496 (2010).
12. Liao, L. *et al.* High- κ oxide nanoribbons as gate dielectrics for high mobility top-gated graphene transistors. *PNAS*. **107**, 6711–6715 (2010).
13. Farmer, D. B. *et al.* Utilization of a Buffered Dielectric to Achieve High Field-Effect Carrier Mobility in Graphene Transistors. *Nano Lett.* **9**, 4474–4478 (2009).
14. Chen, W., Chen, S., Qi, D. C., Gao, X. Y. & Wee, A. T. S. Surface Transfer p-Type Doping of Epitaxial Graphene. *J. Am. Chem. Soc.* **129**, 10418–10422 (2007).
15. Lu, Y. H., Chen, W. & Feng, Y. P. Tuning the Electronic Structure of Graphene by an Organic Molecule. *J. Phys. Chem. B* **113**, 2–5 (2009).
16. Manna, A. K. & Pati, S. K. Tuning the Electronic Structure of Graphene by Molecular Charge Transfer: A Computational Study. *Asian J. Chem.* **4**, 855–860 (2009).
17. Gowtham, S., Scheicher, R. H., Ahuja, R., Pandey, R. & Karna, S. P. Physisorption of nucleobases on graphene: Density-functional calculations. *Phys. Rev. B* **76**, 033401 (2007).
18. Chirayil, T., Zavalij, P. & Whittingham, M. S. Hydrothermal synthesis and characterization of “ $\text{Li}_x\text{V}_{2-\delta}\text{O}_{4-\delta}\cdot\text{H}_2\text{O}$ ”. *Solid State Ionics* **84**, 163–168 (1996).
19. Xiao, Y., Hu, K. A., Yu, Q. C. & Wu, R. J. Preparation of Polyethylene Oxide/ $\text{Li}_x\text{V}_{2-\delta}\text{O}_{4-\delta}$ Nanocomposites. *J. Appl. Polym. Sci.* **60**, 2162–2166 (2001).
20. Li, D., Müller, M. B., Gilje, S., Kaner, R. B. & Wallace, G. G. Processable aqueous dispersions of graphene nanosheets. *Nat. Nanotechnol.* **3**, 101–105 (2008).
21. Bonaccorso, F., Sun, Z., Hasan, T. & Ferrari, A. C. Graphene photonics and optoelectronics. *Nat. Photonics*. **4**, 611–622 (2010).
22. Xue, K. & Xu, Z. P. Strain effects on basal-plane hydrogenation of graphene: A first principles study. *Appl. Phys. Lett.* **96**, 163103 (2010).
23. Dubois, S. M. M., Zanolli, Z., Declerck, X. & Charlier, J. C. Electronic properties and quantum transport in Graphene-based nanostructures. *Eur. Phys. J. B*. **72**, 1–24 (2009).
24. Barbara, P. F., Meyer, T. J. & Ratner, M. A. Contemporary Issues in Electron Transfer Research. *J. Phys. Chem.* **100**, 13148–13168 (1996).
25. Levesque, P. L. *et al.* Probing Charge Transfer at Surfaces Using Graphene Transistors. *Nano Lett.* **11**, 132–137 (2011).
26. Wu, Y. Q. *et al.* Top-gated graphene field-effect-transistors formed by decomposition of SiC. *Appl. Phys. Lett.* **92**, 092102 (2008).
27. Chakraborty, B., Das, A. & Sood, A. K. Formation of p-n junction in polymer electrolyte-top gated bilayer graphene transistor. *Nanotechnology* **20**, 365203 (2009).
28. Kim, B. J. *et al.* High-Performance Flexible Graphene Field Effect Transistors with Ion Gel Gate Dielectrics. *Nano Lett.* **10**, 3464–3466 (2010).
29. William, S., Hummers, J. R. & Offeman, R. E. Preparation of Graphitic Oxide. *J. Am. Chem. Soc.* **80**, 1339 (1958).
30. Kresse, G. & Hafner, J. Ab initio molecular-dynamics simulation of the liquid-metal-amorphous-semiconductor transition in germanium. *Phys. Rev. B* **49**, 14251–14269 (1994).
31. Kresse, G. & Furthmüller, J. Efficiency of ab-initio total energy calculations for metals and semiconductors using a plane-wave basis set. *Comput. Mater. Sci.* **6**, 15–50 (1996).
32. Kresse, G. & Joubert, J. From ultrasoft pseudopotentials to the projector augmented-wave method. *Phys. Rev. B* **59**, 1758–1775 (1999).
33. Dudarev, S. L. *et al.* Electron-energy-loss spectra and the structural stability of nickel oxide: An LSDA1U study. *Phys. Rev. B* **57**, 1505–1509 (1998).
34. Ceperley, D. M. & Alder, B. J. Ground State of the Electron Gas by a Stochastic Method. *Phys. Rev. Lett.* **45**, 566–569 (1980).
35. Giovannetti, G., Khomyakov, P. A., Brocks, G., Kelly, P. J. & Brink van den, J. Substrate-induced band gap in graphene on hexagonal boron nitride: Ab initio density functional calculations. *Phys. Rev. B* **76**, 073103 (2007).
36. Liebsch, A., Ishida, H. & Bihlmayer, G. Coulomb correlations and orbital polarization in the metal-insulator transition of VO_2 . *Phys. Rev. B* **71**, 085109 (2005).
37. Neugebauer, J. & Scheffler, M. Adsorbate-substrate and adsorbate-adsorbate interactions of Na and K adlayers on Al(111). *Phys. Rev. B* **46**, 16067–16080 (1992).

Acknowledgements

This work was financially supported by the National Basic Research Program of China (No. 2009CB939901 and No. 2011CB921404), National Natural Science Foundation of China (No. 11079004, 10979047, 90922016), and innovation project of Chinese Academy of Science (KJCX2-YW-H2O).

Author contributions

H.O.Z., Y.X. and J.L.Y. conceived the idea and co-wrote the paper. X.S. supported assembling the device. X.M.Q. carried out the theoretical calculations. NEXAFS spectra were recorded and interpreted by W.S.Y. All the authors discussed the results, commented on and revised the manuscript.

Additional information

Supplementary information accompanies this paper at <http://www.nature.com/scientificreports>

Competing financial interests: The authors declare no competing financial interests.

License: This work is licensed under a Creative Commons Attribution-NonCommercial-No Derivs 3.0 Unported License. To view a copy of this license, visit <http://creativecommons.org/licenses/by-nc-nd/3.0/>

How to cite this article: Zhu, H.O. *et al.* Rocking-Chair Configuration in Ultrathin Lithium Vanadate-Graphene Hybrid Nanosheets for Electrical Modulation. *Sci. Rep.* **3**, 1246; DOI:10.1038/srep01246 (2013).